Arabian Journal of Geosciences (2019) 12: 108
https://doi.org/10.1007/s12517-019-4246-y

ORIGINAL PAPER

Effect of tunnel overburden stress on the rock brittle failure depth

Heyam H. Shaalan[1] · Mohd Ashraf Mohamad Ismail[1] · Romziah Azit[2]

Received: 11 September 2017 / Accepted: 11 January 2019 / Published online: 5 February 2019

Abstract
Tunneling under high overburden stresses results in many tunnel instability problems due to the rock overstressing. Understanding and simulating the rock failure process is the major issue of a deep excavation to achieve an appropriate rock support system that provides possible cost-effective and stable construction. The excavation of the Pahang Selangor Raw Water Transfer Tunnel is considered in this paper. Three critical cases of the project are analyzed. A possible rock brittle failure was predictable at the tunnel sidewalls under a depth of more than 500 m. The rock overstressing is analyzed based on the in situ stress conditions, intact rock strength, and actual failure depth observed at the site. Failure zones are simulated using the cohesion softening–friction hardening model and compared with the site observed failures. A review of underground openings excavated in different rock mass conditions showed that the ratio of the maximum boundary stress to the uniaxial compressive strength ($\sigma_{\theta\max}/\sigma_{ci}$) is suggested as the key parameter to determine the tunnel instability problems. In this study, an attempt is made to investigate the influence of the maximum tangential boundary stress to the uniaxial compressive strength ratio($\sigma_{\theta\max}/\sigma_{ci}$) on the rock brittle failure depth, stress distribution, and displacement of the rock mass around the tunnel. A parametric study is implemented using different tunnel depths including the actual tunnel depths. The results show that with increasing tunnel depth or ($\sigma_{\theta\max}/\sigma_{ci}$) ratio, the risk of spalling, rock burst, and other tunnel instabilities are increasing.

Keywords Rock spalling · Cohesion softening–friction hardening model · Tunnel stability · Shotcrete lining · Numerical modeling

Introduction

Nowadays, due to the development of construction technology and the need for deep underground excavations, tunneling under highly overburdened ground continue to increase. The excavation of the underground opening causes new sets of stresses and deformation around the opening. Therefore, different instability problems may occur, such as ground squeezing, rock burst, or rock swelling because of the induced stresses (Sulem et al. 1987; Gong et al. 2012; Ortlepp 2001; Jacobi 1966). The most important concern in the design and construction of tunnels and underground openings is the evaluation of stress and deformation that may generate during or after construction. Tunnel excavation at a great depth of more than 500 m is known as deep excavations. As the depth of excavation increases, tunnel instabilities increase, such as high in situ stresses and earth temperatures, complicated geological condition, and high water flows (Yu et al. 2012). In this case, the risk of rock burst increases with difficult tunnel maintenance, consequently, reduction of the underground safety, productivity, and economic benefits. The major factor that affects deep constructions safety is the high in situ stress. Many serious problems may arise due to high in situ stresses such as large deformation and failure around the tunnel. Reducing these issues is costly and challenge even with hard rock support system (Yu et al. 2012). In hard rock tunneling, failure is dependent on the in situ stress magnitude and the rock mass conditions.

The failure process at low in situ stress is dominated by the continuity and discontinuity of the rock mass neutral fractures. At high in situ stresses, the failure is controlled by new stress-induced fractures growth parallel to the excavation boundary. This fracture is known as a brittle failure (Martin et al. 1999).

✉ Mohd Ashraf Mohamad Ismail
ceashraf@usm.my

Heyam H. Shaalan
heyamshaalan89@gmail.com

Romziah Azit
Romziah71@gmail.com

[1] School of Civil Engineering, Universiti Sains Malaysia, Engineering Campus, 14300 Nibong Tebal, Pulau Pinang, Malaysia

[2] Centre of Excellence for Technology and Engineering (CREaTE), Jabatan Kerja Raya, Kuala Lumpur, Malaysia

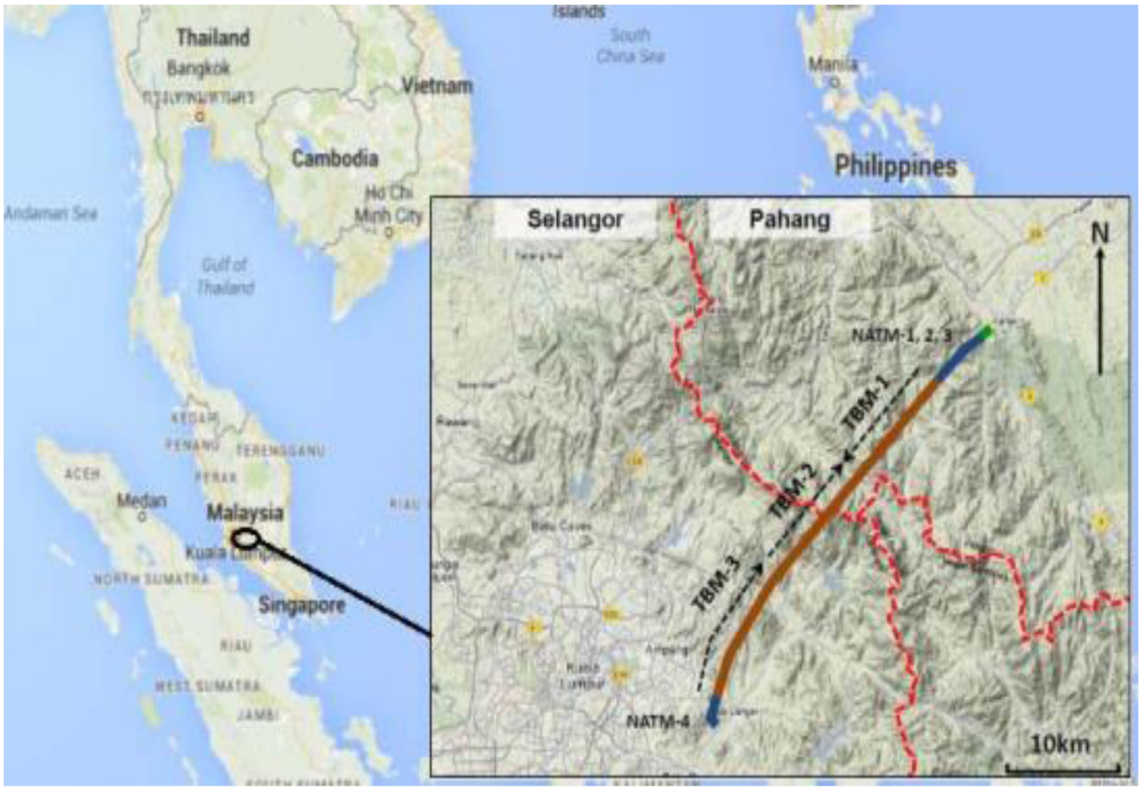

Fig. 1 Structure of Pahang Selangor Raw Water Transfer tunnel (Azit and Ismail 2016)

The confining stress on the tunnel boundary is decreased due to excavation process, whereas in the anisotropic stress filed causes the tangential stresses to increase (Martin et al. 1997). The failure process initiation occurs due to the tensile failure propagation of pre-existing crack tips; thus, the friction is confined and only relevant for small-scale strength (i.e., grain boundary structures and internal cleavage planes) (Diederichs 2007). The plastic zone is formed when tangential stresses at the excavation boundary are more than half of the rock compressive strength. In deep excavation, maximum stress at the tunnel boundary can cause brittle failure in form of spalling especially when it exceeds rock mass strength. Rock spalling

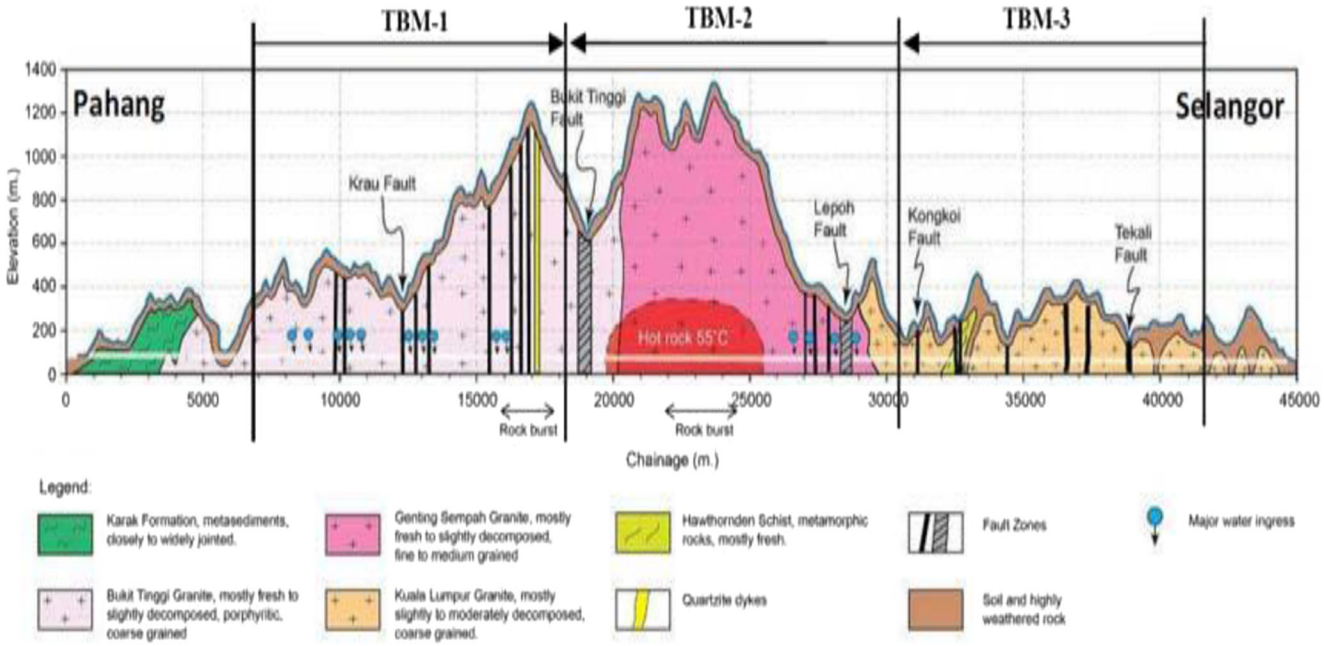

Fig. 2 Geological profiles along tunnel and TBM excavation location (Kawata et al. 2014)

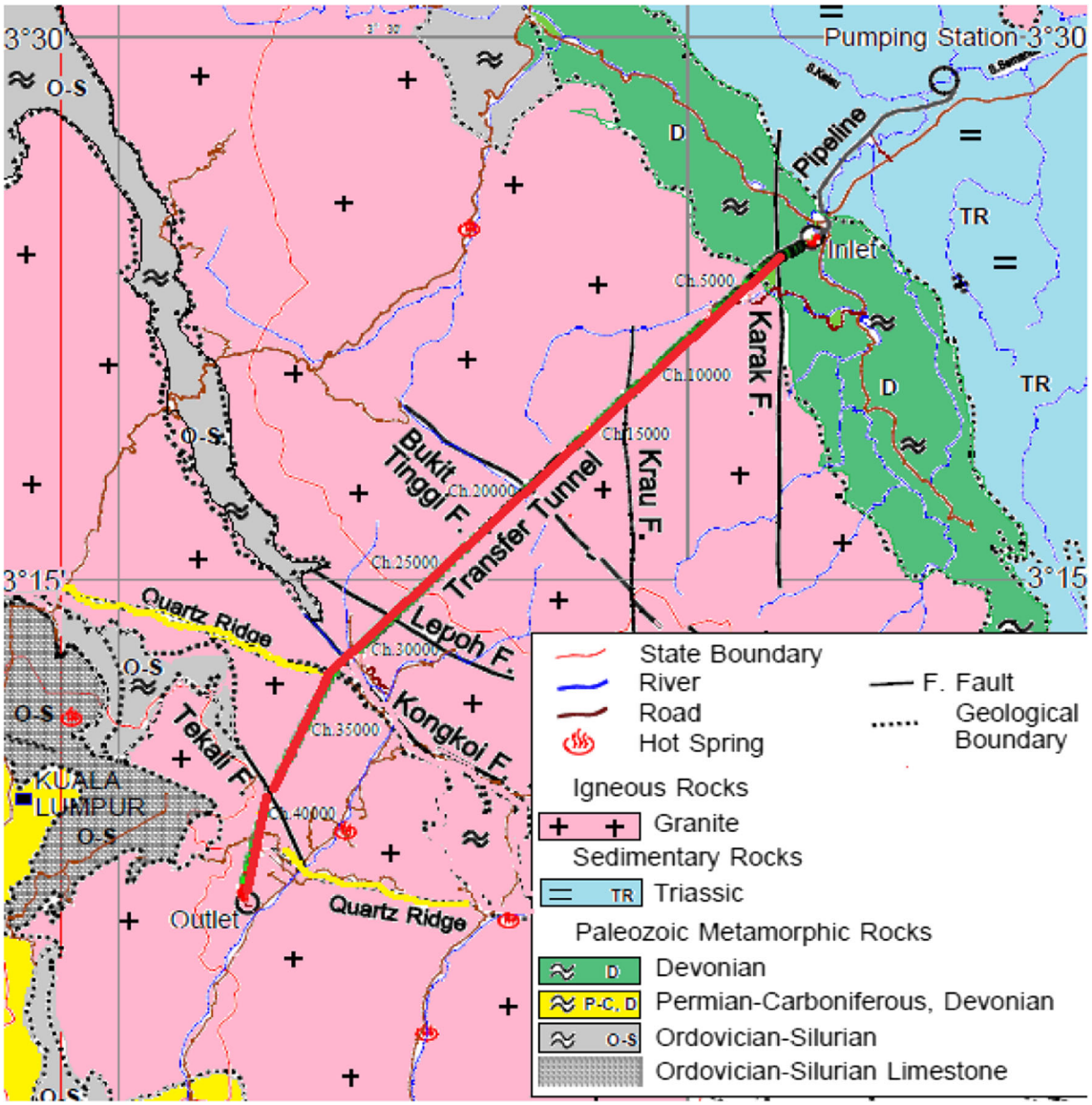

Fig. 3 Geological condition of the project

can be defined as the development of visible extension fractures under compressive loading near the excavation boundary. The direction of spalling fractures is normally parallel to the direction of major principal stress (Hamdi et al. 2015). In addition, the rock spalling is a mode of damage and overbreak in hard rocks around deep tunnels. Spalling occurs as a violent compressive stress causes cracks to grow behind the excavated surface and buckling of thin rock slabs. The intensity of spalling varies from minor spalling to complete collapse of an excavated surface (Andersson 2007). It may occur shortly

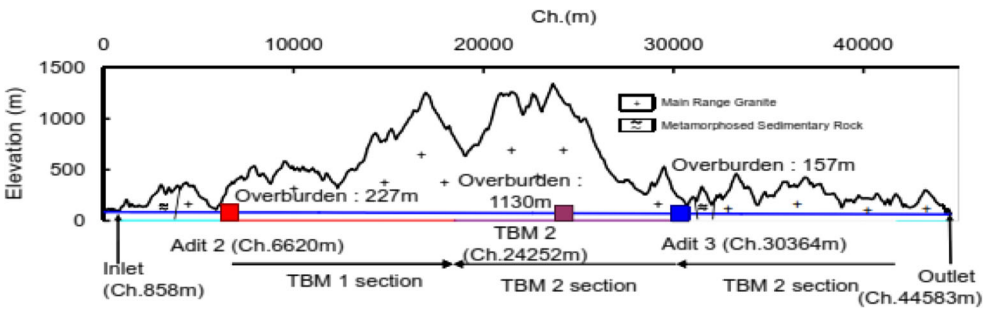

Fig. 4 In situ stress test locations in Pahang Selangor Water Transfer Tunnel (Azit et al. 2015)

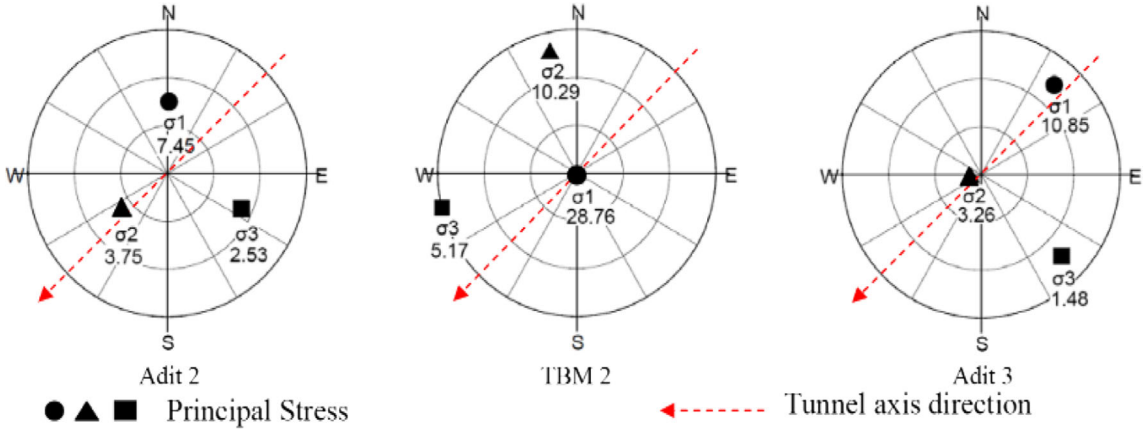

Fig. 5 Projection of principal stress (Azit et al. 2015)

after excavation and extends to form notch, wedges, and fracturing. Thus, the reinforcement must apply immediately after excavation to get a stable structure. To secure deep underground openings under high stresses, it is essential to use a support with a larger energy-absorbing capacity and a good surface coverage. Steel fiber reinforced shotcrete lining is one of tunnel supports which achieves those requirements. Shotcrete with the steel fiber demonstrates the ductile behavior and the efficiency to absorb a significant amount of energy in case of large deformations, but the plain shotcrete is rather brittle (Vandewalle 1998). In addition, there are many rock support systems have been suggested by researchers for deep constructions subjected to high stresses, such as rock bolts, wire mesh, and cable bolts (Hoek et al. 1995). There are many technics applied to reduce the rock failure depth and increase the tunnel stability. The effect of an excavation shape, size, and the magnitude of the stresses on the stability has been investigated. Hoek and Brown (Hoek and Brown 1980) showed that optimizing the layout shape of a cavern can effectively decrease the required rock support. Rock support should be able to hold the weight of the predicted rock spalling region. Shaalan et al. (Shaalan et al. 2017) indicated that the rock brittle failure depth could be decreased by decreasing the tunnel lining thickness, tunnel diameter, as well as rock scaling. In this paper, the influence of the maximum tangential boundary stress to the uniaxial compressive strength ratio($\sigma_{\theta max}/\sigma_{ci}$) on the rock brittle failure depth, stress distribution, and the total displacement of the rock mass around the tunnel is investigated. Three critical cases of TBM-2 section of the Pahang Selangor Raw Water Transfer project are studied. These cases suffered from rock spalling up to 0.3–0.6 m deep at the tunnel sidewalls which is damaged the steel fiber reinforced shotcrete (SFRS) lining. The failure around the tunnel is simulated using a cohesion softening–friction hardening (CSFH) material model. A parametric study is performed using different tunnel depths to indicate their effect, in term of ($\sigma_{\theta max}/\sigma_{ci}$)ratio, on the simulated failure zone.

Project background

Pahang Selangor Raw Water Transfer project is in the central zone of Peninsular Malaysia with 44.6 km long and 5.2 m diameter, as shown in Fig. 1. This project used to transfer

Table 1 Summary of in situ stress test

Item	Adit 2	TBM-2	Adit 3	Unit
Chainage	6620	24,252	30,364	m
Overburden	227	1130	157	m
Vertical stress	4.7	28.2	3.6	MPa
Horizontal stress	6.4	10.8	10.8	MPa
Lateral stress ratio k (σ_h/σ_v)	1.4	0.3	0.3	–
Maximum principal stress σ_1	7.45	28.76	10.85	MPa
Medium principal stress σ_2	3.75	10.29	3.26	MPa
Minimum principal stress σ_3	2.53	5.17	1.48	MPa
Maximum principal stress direction	34.9	80.22	14.2	°

Fig. 6 Rock overstressing at the Pahang Selangor Raw Water Tunnel **a** at 1050 m (Ch. 16,300 m), **b** at 130 m (Ch. 24,610) (Azit et al. 2015)

raw water through a transfer tunnel from a river in Pahang state to Selangor state. Its function is to provide about 1.89 billion liters of water per day to the state of Selangor and the Federal Territories of Kuala Lumpur and Putrajaya. Consequently, it relieved the shortage of water supply for daily life and industries. It is one of the largest infrastructure projects in Asia. The tunnel was excavated using three TBMs (TBM 1, TBM 2, and TBM 3) for about 35 km of the whole tunnel length by 1200 m deep. The conventional tunnel excavation method (NATM) has been used to excavate four sections of the total 9.1 km long while the cut-and-cover method used to excavate one section of 0.9 km long. The deepest section is 1246 m and about 5000 m of the tunnel has over 1000 m deep (Azit and Ismail 2016). The geological environment along the tunnel consists of granite starting from Ch. 3.9 km until the end of the tunnel (Azit et al. 2015). The average unit weight and Poisson's ratio are 27 KN/m^3 and 0.2, respectively. In this work, the TBM-2 section, particularly Ch. 23,048 m, Ch. 23,732 m and 23,742 m, is selected for the numerical analysis since it is subjected to a possible rock failure (see Fig. 2).

Geological mapping

The geological map of the project is shown in Figs. 2 and 3. The geological environment of the tunnel includes of Kara Formation starting from the entrance until the Ch. 4.0 km which consists of metasediments, such as schist, phyllite, and hornfels. The geological from Ch. 4.0 km to the end of the tunnel made up of granite with small sections of Hawthorndon Schist. The granite is divided into three parts: Bukit Tinggi Granite, Genting Sempah micro-Granite, and Kuala Lumpur Granite. Bukit Tinggi Granite part was porphyritic and coarse grained, mostly fresh to slightly decomposed and cut by the Krau Fault. TBM-1 was used to excavate in that part leading to rock burst at several locations. TBM 2 was utilized to excavate the three granite types, the biggest part being in Genting Sempah micro-granite and passing through two major faults: the Bukit Tinggi Fault and Lepoh Fault. Many instability problems have been arising in TBM-2 section, such as high rock stress, rock burst, and collapsing ground at the extensive fault zones. On the other hand, the Kuala Lumpur Granite part was excavated by TBM-3, with small sections of Hawthorndon Schist and several faults such as the Tekali Fault and Kongkoi Fault. In general, the rock in this part was coarse grained, slightly to moderately decomposed (Kawata et al. 2014). Many faults with a strike have been observed intersected with the tunnel alignments. Particularly, these faults refer to a stress tensional state in the central part of the project. In addition, several lineaments such as stream channels have been indicated by the regional topographic trends. Both faults and lineament seem to be complete parts of the granite position (Azit and Ismail 2016). The grain size of the granite varies fine to coarse with several centimeter orders. Granite can be generally divided into three sections by grain size, coarse grained granite from Ch. 3.9 km to Ch. 20 km, fine grained granite from Ch. 20 km to 29 km, and medium grained granite from Ch. 29 km to the outlet. The quartz content is ranging from 25 to 40% based on a drill core sample of BH.

Table 2 Field observed failures

Cases	Chainage (m)	Depth (m)	Field comments from the geological map
1	23,048	1002	Spalling up to 0.3 m deep in the side walls damaged the shotcrete lining
2	23,732	1241	Spalling occurred in the tunnel walls up to 0.6 m deep and damaged the shotcrete
3	23,742	1239	Spalling occurred in the tunnel walls up to 0.5 m deep and damaged the shotcrete lining

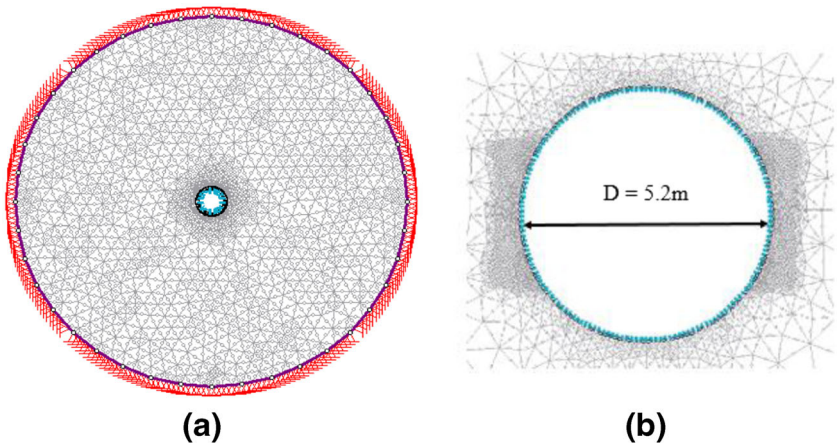

Fig. 7 **a** Geometrical model; **b** meshing around the tunnel

In situ stress conditions

The in situ stress conditions along the tunnel have been evaluated, and a series of initial stress measurements is performed at various locations along the tunnel to establish the magnitude and direction of the stresses in rock mass as in Figs. 4, 5. Both of hydraulic fracturing and compact conical-ended borehole overcoring (CCBO) methods have been employed to investigate magnitudes and orientations of the in situ stresses. The results of the Compact Conical-ended Borehole Overcoring (CCBO) test are used for the current study. CCBO method was applied to measure three-dimensional in situ stress in a single borehole. The initial stress is measured from twenty-four (24) strain gauges. For the in situ CCBO test, borehole for the testing was 76 mm diameter and was drilled more than 10 m' distance from the tunnel wall. Based on the results of the drilled borehole, its calculations derived the initial stress tensor composed of six (6) stress components and then converted to the principal stress in three-dimensional, as shown in Table 1. The high in situ stresses have been observed in the center of the mountain, especially in TBM-2 section. The maximum principal stress (σ1) is recorded along the vertical direction. On the other hand, the horizontal stress σ_h is comparatively small, so its ratio to vertical stress σ_v is 0.38 (Azit et al. 2015).

Based on the field observation, many rock failures were occurred during the tunnel construction in form of rock burst and spalling. Spalling is described as the compressive stress-induced slabs formed on the boundary of an underground opening and resulting in breakouts or V-shaped notch in the region of maximum tangential stress, while rock burst is a sudden and violent failure of rock overstressed resulting in a rapid release of a large amount of accumulated energy. In another word, the spalling is light rock burst. At the site, due to high stresses, rock failures have occurred at tunnel sidewalls while the crown was not affected, as shown in Fig. 6. In fact, the rock geological structure had no effect on the failures generation (Kawata et al. 2014). The filed observed failures for the three critical cases, used in this study, are presented briefly in Table 2.

Table 3 Rock compressive strength form Schmidt hammer test

Cases	UCS (MPa)	RQD
1	124	75%
2	94	70%
3	118	75%

Methodology

Analysis of the rock overstressing

Normally, rock mass is in a state of equilibrium but tunneling changes the in situ stress state, leading to new sets of stresses and deformation around the opening. Maximum stress concentrates around tunnel openings is known as a maximum tangential stress, which is calculated using the Kirsch equation (Kirsch 1898), referring to the following equations:

$$\sigma_r = \frac{P_1 + P_2}{2}\left(1-\frac{a^2}{r^2}\right) + \frac{P_1-P_2}{2}\left(1-\frac{4a^2}{r^2}+\frac{3a^4}{r^4}\right)\cos 2\theta \quad (1)$$

$$\sigma_\theta = \frac{P_1 + P_2}{2}\left(1+\frac{a^2}{r^2}\right) - \frac{P_1-P_2}{2}\left(1+\frac{3a^4}{r^4}\right)\cos 2\theta \quad (2)$$

$$\tau_{r\theta} = -\frac{P_1-P_2}{2}\left(1+\frac{2a^2}{r^2}-\frac{3a^4}{r^4}\right)\sin 2\theta \quad (3)$$

Table 4 Input parameters of the numerical modeling

Input parameters for RockLab				
Term	Unit	Case 1	Case 2	Case 3
Intact compressive strength σ_{ci}	MPa	124	94	118
Material constant for intact rock m_i	–	32	32	32
Disturbance factor D	–	0	0	0
Geological strength index GSI	–	67	60	67
Modulus ratio MR	–	425	425	425
Unit weigh γ_d	KN/m^3	27	27	27
Tunnel depth	m	1002	1241	1239
Output parameters for RockLab				
Young modulus E	MPa	35,516	20,774	33,798
Rock mass compressive strength σ_{cm}	MPa	19.7	10.06	18.74
Rock mass tensile strength σ_t	MPa	0.322	0.144	0.306
Friction angle $\varnothing_m$	°	52	47	51
Cohesive strength C_m	MPa	6.239	5.75	6.96
m_b	–	9.84	7.66	9.84
s	–	0.026	0.011	0.025

where σ_r is the radial stress (MPa), σ_θ is the tangential stress (MPa), τ_r is the shear stress around the tunnel (MPa), P_1 and P_2 are σ_v, and σ_h which are the vertical and horizontal stresses, respectively (MPa). In addition, a is the tunnel radius (m), r is the distance from the tunnel cross-section center (m), θ is the counterclockwise angle from the spring line of the right sidewall, and k is the coefficient of lateral stress (Goodman 1989). Substituting ($a = r$) in "Eq. (1)" gives the radial stress and shear stress are both zero since this is a free surface. The locations of the maximum stresses along the right and left sides of the wall are 0° and 180°, which are presented by θ. Spalling is a stress-induced failure process; thus, the stresses on the boundary of the excavation and the maximum boundary stress should be evaluated. The maximum tangential stress at the sidewall ($\theta = 0°$ and 180°) is simplified and calculated by Eq. (4):

$$\sigma_{\theta\ \max} = 3\sigma_v - \sigma_{\mathrm{hmin}} \tag{4}$$

Table 5 Steel fiber reinforced shotcrete lining properties

Item	Unit	Value
Young modulus$E$	MPa	23,900
Poisson ratio ν	–	0.2
Uniaxial compressive Strength $f_{c,\,3}$	MPa	25.5
Tensile strength $f_{t,\,3}$	MPa	2.55[1]
Steel fiber content	kg/m^3	35
Lining thickness	m	0.1

[1] Assumption: $f_{t,\,3} = 0.1 f_{c,\,3}$ (Saurer et al. 2014)

whereσ_θ = tangential stress, σ_v = vertical stress, and σ_{hmin} = minimum horizontal stress.

The ratio of the maximum boundary stress to the uniaxial compressive strength ($\sigma_{\theta\max}/\sigma_{ci}$) is suggested as the key parameter to determine the tunnel instability risks. Based on the site observation collected by Hoek and Brown (Hoek and Brown 1980), Martin et al. (Martin et al. 1999) showed that increasing the ratio of the maximum boundary stress to the uniaxial compressive strength ($\sigma_{\theta\max}/\sigma_{ci}$) makes the stability of the tunnel very difficult to achieve. Furthermore, Hoek and Marinos (Hoek and Marinos 2009) suggested an overstressing classification based on personal observations from the results provide by Hoek and Brown (Hoek and Brown 1980) and Martin et al. (Martin et al. 1999). They conducted that the ratio of maximum tangential stress to rock uniaxial compressive strength($\sigma_{\theta\max}/\sigma_{ci}$) = 0.45 for minor spalling, 0.6 for moderate spalling, 0.9 for severe spalling, 1.2 for extreme spalling, and 1.6 for possible rock bursts.

Numerical modeling

Field data from a real project based on Pahang Selangor Raw Water Transfer Tunnel are collected. A numerical analysis is performed using Rocscience RS2 (version: 9.0). It is the most widely applied software for rock mechanics issues due to its flexibility treatment with the material heterogeneity, nonlinear deformation, in situ stresses, and gravity (Rocscience Inc. 2012). To reduce the element number, a circular domain is used around the tunnel opening (Edelbro 2010), as shown in Fig. 7. In the modeling, an expansion factor is used in

Table 6 Tunnel depths for the stability analysis

Case 1		Case 2		Case 3	
Tunnel depth (m)	$(\sigma_{\theta max}/\sigma_{ci})$	Tunnel depth (m)	$(\sigma_{\theta max}/\sigma_{ci})$	Tunnel depth (m)	$(\sigma_{\theta max}/\sigma_{ci})$
1002	0.65	1241	0.86	1239	0.68
900	0.52	900	0.69	900	0.55
800	0.46	800	0.61	800	0.48
700	0.4	700	0.53	700	0.42

determining how far an automatically generated external boundary can be projected relative to a given excavation dimension. Expansion factor is set to 6.5 to decrease the boundary effects. Triangular elements with six nodes are utilized for the finite element mesh. Mesh densities in the critical areas of the model (e.g., around excavations) can be increased without affecting the mesh outside of these regions. Increasing mesh density close to the excavation boundary results in more obvious and distinct shear. The location of the failure zone is dependent on the element size. Therefore, larger elements size leads to wider and more diffuse shear bands (Edelbro 2010). In this analysis, an extremely fine mesh density (gradation factor of 0.1) is used in the critical area located on the tunnel sidewalls.

RockLab software is used to determine the rock properties by fitting the Mohr-Coulomb failure envelope with the Hoek-Brown failure envelope. The intact compressive strength in the tunnel wall was investigated at the site using Schmidt hammer test (see, Table 3). The properties of the rock mass around the tunnel used in the RockLab are listed in Table 4. The value of material constant for intact rock m_i is determined based on the mineralogy, composition, and grain size of the intact rock (Hoek et al. 1992). Disturbance factor *D*describes the condition of the rock mass. Disturbance of the rock mass results from heavy blast damaged effects as well as stress relief due to the overburden removal. Hoek et al. (Hoek et al. 2002) provided guidelines for estimation the disturbance factor *D*. For the current project, disturbance factor *D*is 0 since excavation by TBM results in minimum rock mass disturbance around the tunnel. Hoek et al. (Hoek et al. 2013) presented a suggested quantification of the GSI chart based on two well-established parameters, Joint Condition and RQD, as shown in "Eq. (5)." $JCond_{89}$ and RQD scales are used to represent the discontinuity surface conditions and the blockiness of the rock mass. Surface conditions of the current cases are good, rough, and slightly weathered.

$$GSI = 1.5\ JCond_{89} + RQD/2 \tag{5}$$

The rock mass modulus *E* could be estimated using modulus ratio MR which can be selected by the rock type. Mohr-Coulomb model is used to simulate the rock mass behavior.

The total field stress is applied in a single phase by default for numerical modeling. In fact, this technique is relevant especially when no mining effect is observed in the rock mass. Therefore, the stress must be applied gradually with many stages to involve the mining process effect (Edelbro 2008). A multistage analysis is implemented to simulate the tunnel excavation process. The load split option is applied for the said purpose, in which the user can split the field stress-induced load between any model stage rather than applying the entire load in a single phase. Using this option, the tunnel material is removed immediately at the first stage, while the in situ stresses are applied gradually in stages as a boundary condition until reaching the in situ stress state. In addition, the load split option is performed to simulate the 3D effect of an advancing tunnel face, using a 2D model. Eight stages with 12.5% of the total in situ stress at each stage are applied to the model boundary.

Tunnel support

The tunnel has been supported using steel fiber reinforced shotcrete lining SFRS. The properties of the SFRS lining are listed in Table 5. The function of SFRS is to ensure the stability of the tunnel by controlling the deformation and spalling caused by the overstressing. The compressive strength and Poisson ratio of the shotcrete has been obtained from shotcrete

Table 7 Rock failure classification

Case	$(\sigma_{\theta max}/\sigma_{ci})$	Failure classification
1	0.65	Moderate spalling
2	0.86	Moderate to severe spalling
3	0.68	Moderate spalling

Table 8 Input parameters of CSFH model

Case	c_{peak}	$\varnothing_{peak}$	$c_{residual}$	$\varnothing_{residual}$
1	21.14	16	6.34	52
2	18.58	15	5.57	47
3	21.2	10	6.36	51

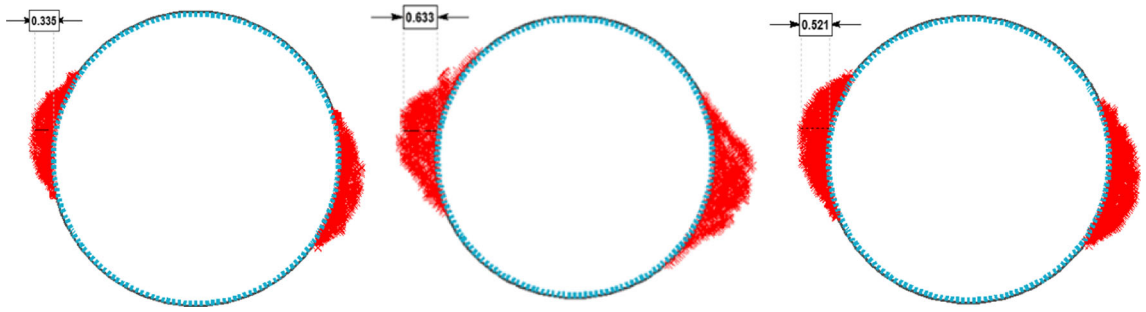

Fig. 8 Simulated failure zone of the tunnel sidewalls using CSFH model (m)

samples test that made during tunnel construction. The young modulus of the shotcrete lining is calculated according to ACI 318-08 (ACI 318-08 2008). The lining thickness is about 100 mm.

Numerical simulation of the rock failure

A CSFH material model is applied to simulate the observed rock failure at tunnel sidewalls under high stresses. It is an elastic-brittle-plastic model presented by Edelbro (Edelbro 2010) and can best capture the actual rock failure. The CSFH model shows suitable results for hard rock masses when predicting the failure observed in the field (Hajiabdolmajid et al. 2002; Diederichs et al. 2004). Using the elastic-brittle-plastic with the CSFH model, the cohesion decreases, and the friction increases instantaneously in residual values after peak strength is exceeded (Edelbro 2008). In addition, the material behavior can be modeled based on peak and residual parameters evaluation of the Mohr-Coulomb failure criterion (Hoek et al. 1992). Yield elements failed in shear are used as failure indicators. The strength parameters of the CSFH model are evaluated based on the equations provided by Edelbro (Edelbro 2010). The peak cohesion strength can be calculated as follows:

$$c_{\text{peak}} = \frac{\sigma_{cm}(1-\sin\varnothing_m)}{2cos\varnothing_m} \tag{6}$$

where σ_{cm} is the compressive strength of the rock mass, while φ_m is the friction angle of the rock mass and can be obtained using Rock Lab as shown in Table 4. The peak friction angle φ_{peak}value when utilizing CSFH model is between 0 and 22° as suggested by Hajiabdolmajid (Hajiabdolmajid et al. 2002) and Diederichs (Diederichs et al. 2004). Based on this study, Hajiabdolmajid et al. (Hajiabdolmajid et al. 2002) indicated that a peak friction angle equal to zero leads to a very wide and deep zone of yielded elements. Furthermore, a parametric study was carried out by Shaalan et al. (Shaalan et al. 2017) to show the effect of peak friction angle φ_{peak}on the rock failure zone using the range of (0–22°). They found that the variation in the peak friction angle of the CSFH model largely influences the failure shape and depth. The extent and depth of the yield elements that failed in the shear for lower peak friction angles are higher than those obtained from the higher peak friction angles. The residual cohesion strength and friction angle can be calculated according to "Eq. (7)" and "Eq. (8)," respectively.

$$c_{\text{residual}} = 0.3\ c_{\text{peak}} \tag{7}$$

$$\varnothing_{\text{residual}} = \varnothing_{\text{m}} \tag{8}$$

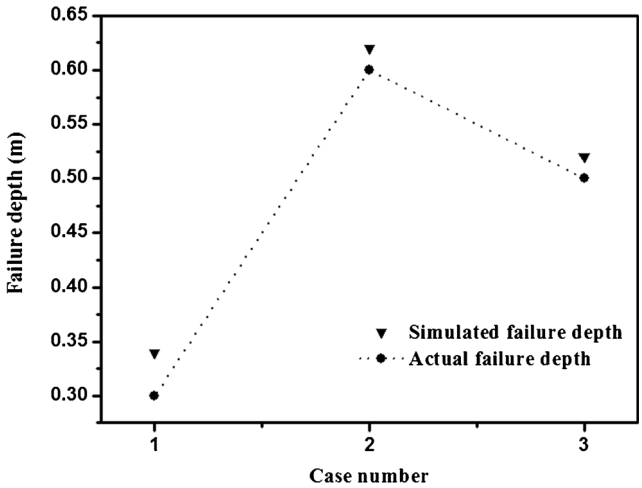

Fig. 9 Comparison between actual and simulated failure depth

Table 9 Actual and simulated failure depth

Case	Actual failure depth (m)	Simulated failure depth (m)
1	0.3	0.34
2	0.6	0.63
3	0.5	0.52

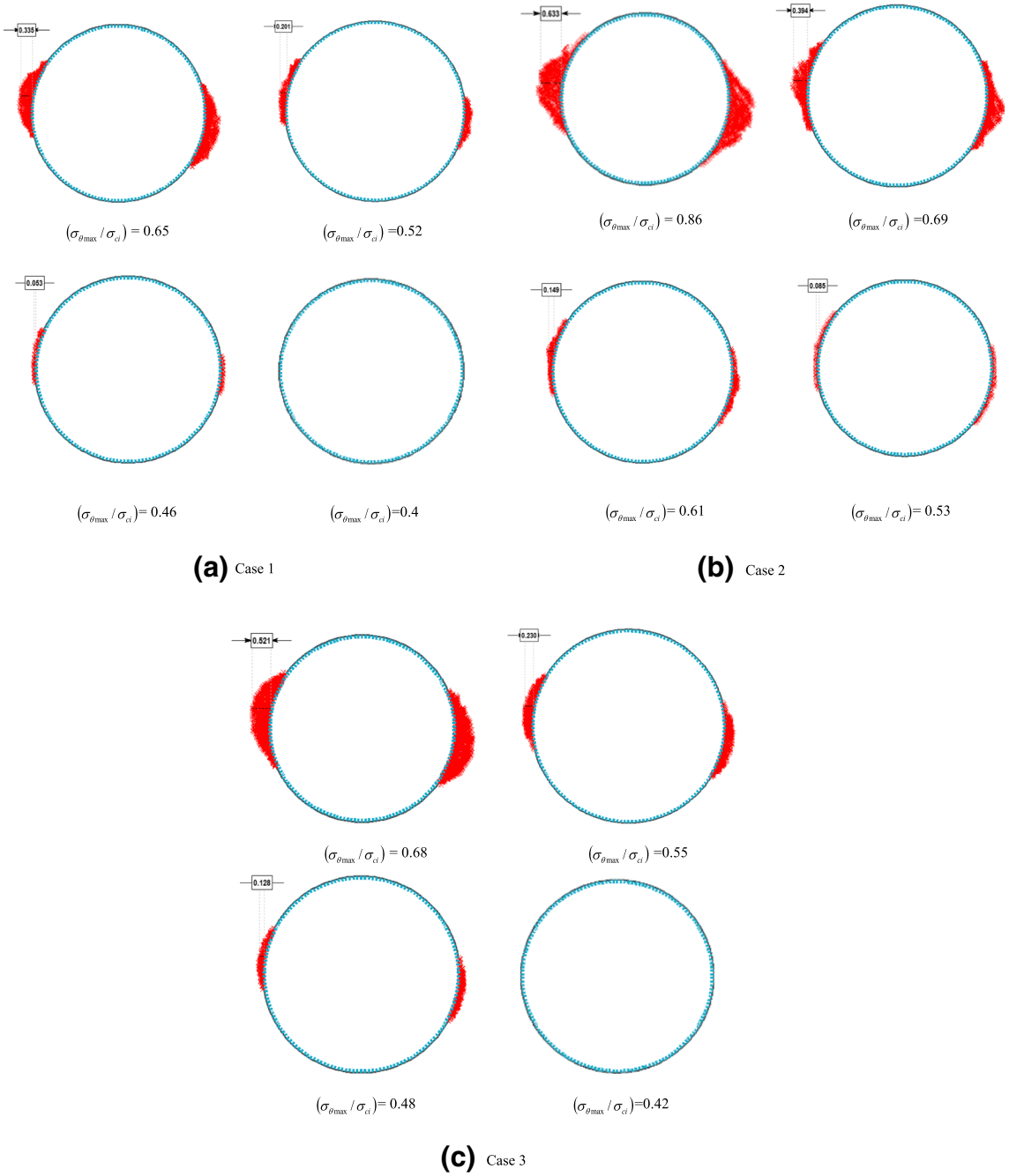

Fig. 10 Distribution of yield element failure in shear under different tunnel depths

Parametric analysis

To assess the tunnel stability and reduce the failure depth around the tunnel, the influence of the tunnel depth in term of the maximum tangential boundary stress to the uniaxial compressive strength ($\sigma_{\theta max}/\sigma_{ci}$)ratio on the simulated failure depth, stress distribution, and displacement of the rock mass is investigated. For the said purpose, four tunnel depths including the actual tunnel depths are adopted as shown in Table 6. Vertical stress σ_v is calculated as expressed in Eq. (9). Horizontal stress σ_h is obtained by multiplying the coefficient of lateral stress k by the vertical stress σ_v as shown in Eq. (10). The maximum tangential stress at the sidewall is calculated by Eq. (4):

$$\sigma_v = \gamma_d \, x \, H \tag{9}$$

$$k = \frac{\sigma_h}{\sigma_v} \tag{10}$$

where σ_v is vertical stress (MPa), γ_d is rock unit weight (MN/m^3), H is tunnel depth (m), k is the coefficient of lateral stress, and σ_h is the horizontal stress.

Numerical results

Estimation of rock spalling

According to "Eq. (4)" and in situ stresses, the maximum tangential stress $\sigma_{\theta max}$ is 81 MPa, which is lower than the rock compressive strength of the three cases (see, Table 3), so the risk of rock burst in the critical cases is low. However, based on the overstressing classification provided by Hoek and Marinos (Hoek and Marinos 2009), a possible rock spalling can occur as shown in Table 7.

Simulated failure zone

The failure zones of the three cases are simulated using the CSFH material model. The strength parameters of the CSFH model for the three cases are presented in Table 8. The peak cohesion c_{peak}, residual cohesion $c_{residual}$, and residual friction angle $\varnothing_{residual}$ are calculated based on Eq. (6, 7, 8), respectively. The peak friction angles $\varnothing_{peak}$ are selected based on the parametric study performed by Shaalan et al. (Shaalan et al. 2017). The simulated failure zones are shown in Fig. 8. The comparison between the simulated and actual failure depths is shown in Fig. 9 and Table 9. The good agreement with field observations shows the efficiency of the CSFH model to predict rock brittle failure in numerical simulations.

Effect of tunnel overburden stress

The effect of tunnel overburden stress in term of $(\sigma_{\theta max}/\sigma_{ci})$ ratio on the simulated failure depth and stress distribution is investigated using four different values of tunnel depths as shown in Table 6. The actual tunnel depths for the three cases are used to compare with other depths. Figure 10 presents the distribution of yield elements failed in shear around the tunnel at different $(\sigma_{\theta max}/\sigma_{ci})$ ratios. It is obvious that the rock failure depth decreases with decreasing the ratio of $(\sigma_{\theta max}/\sigma_{ci})$. At 700 m deep, the yield elements failed in shear disappear for cases 1 and 3 because $(\sigma_{\theta max}/\sigma_{ci})$ ratio is about 0.4. Whereas, in case 2, the failure still occurs with lower depth since a minor to moderate spalling still occurs at $(\sigma_{\theta max}/\sigma_{ci}) = 0.53$. This may due to the high rock compressive strength $\sigma_{ci}$for cases 1 and 3 which are 124 and 118 MPa, respectively, compared with 94 MPa for case 2. Increasing rock compressive strength σ_{ci}results in decreasing the ratio of the maximum tangential boundary stress to the uniaxial compressive strength$(\sigma_{\theta max}/\sigma_{ci})$. The ratio of $(\sigma_{\theta max}/\sigma_{ci})$ versus the simulated failure depths for the three critical cases is shown in Fig. 11. The stress distribution of the rock mass around the tunnel at different tunnel depths and $(\sigma_{\theta max}/\sigma_{ci})$ ratios is evaluated. Increasing the ratio of $(\sigma_{\theta max}/\sigma_{ci})$ could increase the rock stresses closed to the excavation boundary.

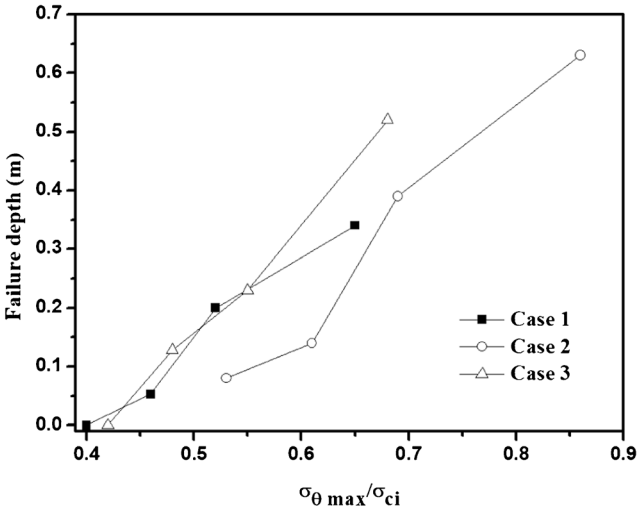

Fig. 11 Effect of tunnel overburden on the rock failure depth

Furthermore, at high tunnel depths, the rock stresses are lower near the tunnel boundary since a brittle failure model is used and the residual strength is primarily governed by the frictional strength (Cai and Kaiser 2014). On the other hand, the maximum principal stresses (tangential stress) will be closed to the tunnel boundary at lower tunnel depths (see, Fig. 12). Figures 13 and 14 show the changes of the ratio of $(\sigma_{\theta max}/\sigma_{ci})$ with the tangential stress and the total displacement of the rock mass, respectively. The total displacement of the rock mass around the tunnel of case 2 is higher than that of cases 1 and 3. However, with increasing the ratio of$(\sigma_{\theta max}/\sigma_{ci})$, the tangential stress and the total displacement of the rock mass are increasing.

Conclusion

Based on the site observation of Pahang Selangor Raw Water Transfer project, rock brittle failures have occurred in the tunnel sidewalls up to 0.3–0.6 m deep and damaged the shotcrete lining. In this study, an analytical method is performed to analyze the tunnel behavior under high overburden stress on the basis of the rock stress-strength relationships and the actual failure. The results indicated that the risk of rock burst is low, but a possible rock spalling could occur. The actual failure zone is simulated using the cohesion softening–friction hardening (CSFH) material model. The good agreement with actual failure depth shows the efficiency of the CSFH model to predict rock brittle failure in numerical simulations. Minimizing rock failure depth around a tunnel can increase the tunnel stability and reduce the amount of the rock support. The ratio of the maximum boundary stress to the uniaxial compressive strength $(\sigma_{\theta max}/\sigma_{ci})$ is suggested as the key parameter to

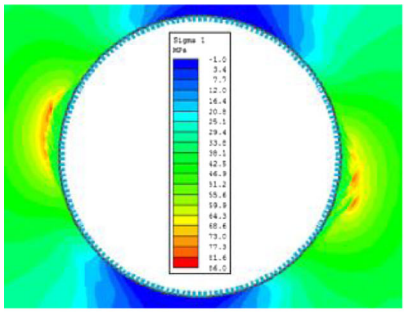

$(\sigma_{\theta max}/\sigma_c) = 0.65$

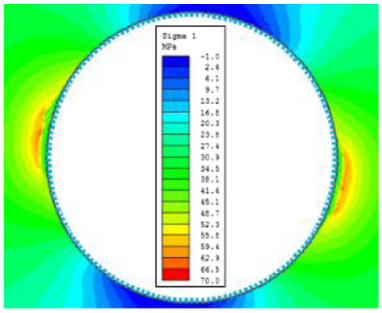

$(\sigma_{\theta max}/\sigma_c) = 0.52$

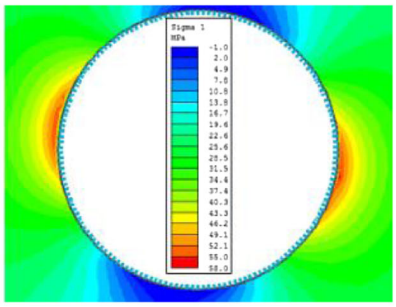

$(\sigma_{\theta max}/\sigma_c) = 0.46$

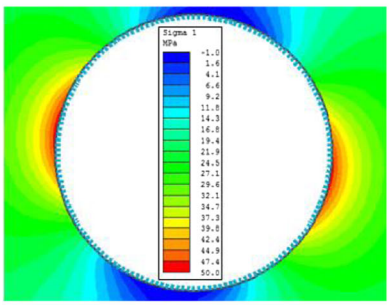

$(\sigma_{\theta max}/\sigma_c) = 0.4$

(a) Case 1

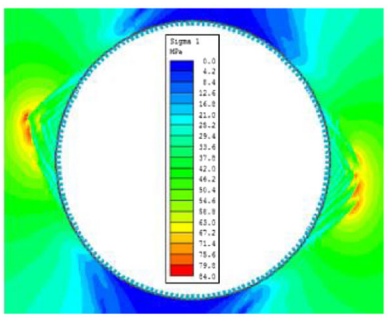

$(\sigma_{\theta max}/\sigma_c) = 0.86$

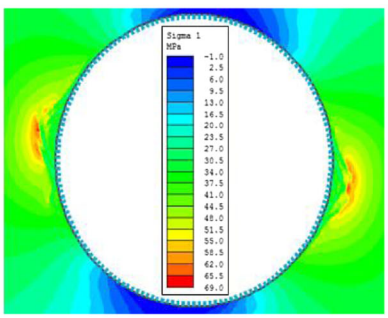

$(\sigma_{\theta max}/\sigma_c) = 0.69$

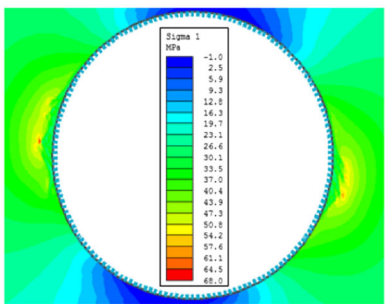

$(\sigma_{\theta max}/\sigma_c) = 0.48$

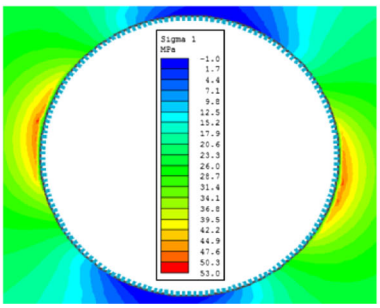

$(\sigma_{\theta max}/\sigma_c) = 0.42$

(b) Case 2

Fig. 12 Stresses distribution of the rock mass around the tunnel at different tunnel depths

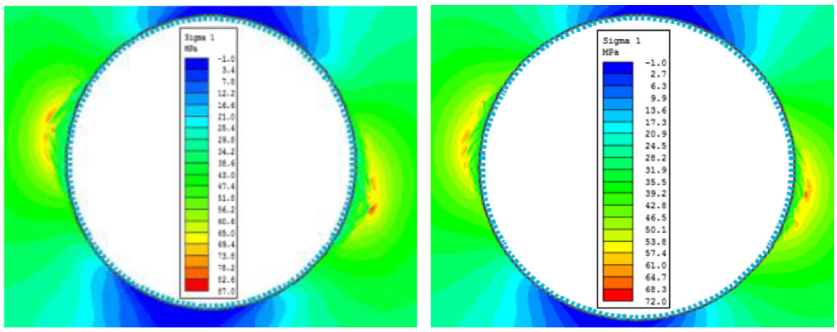

$(\sigma_{\theta max}/\sigma_c) = 0.68$ $(\sigma_{\theta max}/\sigma_c) = 0.55$

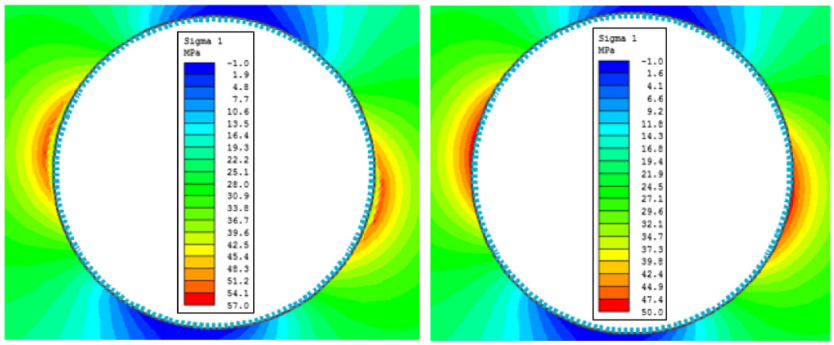

$(\sigma_{\theta max}/\sigma_c) = 0.48$ $(\sigma_{\theta max}/\sigma_c) = 0.42$

(c) Case 3

Fig. 12 (continued)

determine the tunnel instability problems. The effect of the tunnel overburden stress in term of the ratio of ($\sigma_{\theta max}/\sigma_{ci}$) on the simulated failure depth, stress distribution, and the total displacement of the rock mass around the tunnel is evaluated. A parametric study is implemented using different tunnel depths including the actual depths. The results showed that with increasing tunnel depth or ($\sigma_{\theta max}/\sigma_{ci}$) ratio, the risk of rock failure, tangential stresses, and total displacement of the rock mass around the tunnel are increasing.

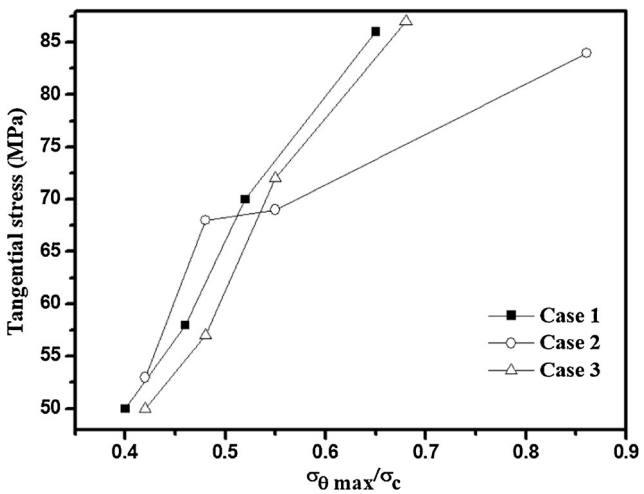

Fig. 13 Effect of tunnel depth on the tangential stress

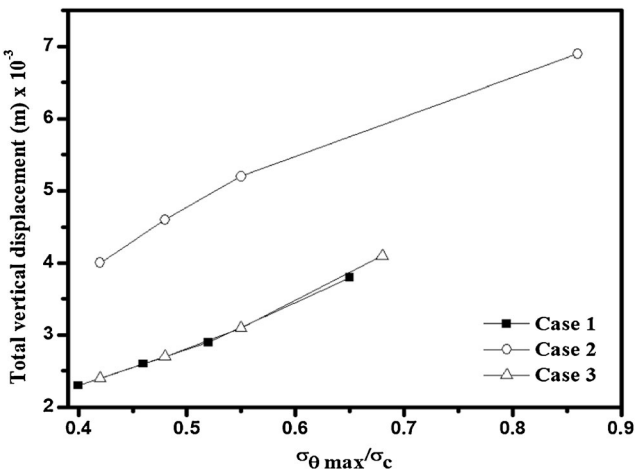

Fig. 14 Effect of tunnel depth on the total displacement of the rock mass around the tunnel

References

ACI 318-08 (2008) Building code requirements for structural concrete and commentary. American concrete institute, Farmington Hills, Michigan, USA

Andersson CJ (2007) Rock mass response to coupled mechanical thermal loading. spö Pillar Stability Experiment. PHD Thesis, KTH, Sweden

Azit R, Ismail MAM (2016) Modeling stress-induced failure for deep tunnel excavation of Pahang-Selangor raw water transfer project. 9thAsian Rock Mechanics Symposium. Bali, Indonesia

Azit R, Ismail MAM, Syed Zainal SF, Mahmood N (2015) Rock overstressing in deep tunnel excavation of Pahang-Selangor raw water transfer project. Appl Mech Mater. https://doi.org/10.4028/www.scientific.net/AMM.802.16

Cai M, Kaiser P (2014) In-situ rock spalling strength near excavation boundaries. Rock Mech Rock Eng 47:659–675. https://doi.org/10.1007/s00603-013-0437-0

Diederichs MS (2007) Mechanistic interpretation and practical application of damage and spalling prediction criteria for deep tunnelling. Can Geotech J. https://doi.org/10.1139/T07-033

Diederichs MS, Kaiser PK, Eberhardt E (2004) Damage initiation and propagation in hard rock during tunnelling and the influence of near-face stress rotation. Int J Rock Mech Min Sci 41:785–812. https://doi.org/10.1016/j.ijrmms.2004.02.003

Edelbro C (2008) Strength, fallouts and numerical modelling of hard rock masses. PHD thesis, Lulea University of Technology Luleå, Sweden

Edelbro C (2010) Different approaches for simulating failure in two hard rock mass cases a parametric study. Rock Mech Rock Eng 43:151–165. https://doi.org/10.1007/s00603-008-0025-x

Gong Q, Yin L, Wu S, Zhao J, Ting Y (2012) Rock burst and slabbing failure and its influence on TBM excavation at headrace tunnels in Jinping II hydropower station. Eng Geol 124:98–108

Goodman RE (1989) Introduction to Rock Mechanics, 2nd edition.. pp 225

Hajiabdolmajid V, Kaiser PK, Martin CD (2002) Modelling brittle failure of rock. Int J Rock Mech Min Sci 39:731–741. https://doi.org/10.1016/S1365-1609(02)00051-5

Hamdi P, Stead D, Elmo D (2015) Characterizing the influence of stress-induced microcracks on the laboratory strength and fracture development in brittle rocks using a finite-discrete element method-micro discrete fracture network FDEM- μ DFN approach. J Rock Mech Geotech Eng. https://doi.org/10.1016/j.jrmge.2015.07.005

Hoek E, Brown ET (1980) Underground excavations in rock. London, England

Hoek E, Marinos P (2009) In: Vrkljan I (ed) Tunnelling in overstressed rock. Rock engineering in difficult ground conditions - soft rocks and karst. Taylor and Francis Group, London, pp 49–60

Hoek E, Wood D, Shah S (1992) A modified Hoek–Brown criterion for jointed rock masses. In: Hudson JA (ed) Rock characterization: ISRM Symposium, Eurock '92, Chester, UK. Thomas Telford, London, pp 209–213

Hoek E, Kaiser PK, Bawden WF (1995) Support of underground excavation in hard rock, vol 1995. Balkema, Rotterdam

Hoek E, Carranza-Torres C, Corkum B (2002) Hoek-Brown failure criterion – 2002 Edition. Proc. North American Rock Mechanics Society meeting in Toronto in July 2002

Hoek E, Carter TG, Diederichs MS (2013) Quantification of the Geological Strength Index chart. 47th US Rock Mechanics / Geomechanics Symposium held in San Francisco, CA, USA

Jacobi O (1966) Occurrence, causes and control of rock dursts in the Ruhr district. Int J Rock Mech Min Sci Geomech Abstr 3:205–219

Kawata T, Nakano Y, Matsumoto T, Mito A, Pittard F, Azman AAS (2014) The relationship between TBM data and rockburst in long-distance tunnel, Pahang-Selangor raw water transfer tunnel, Malaysia. 8th Asian rock mechanics symposium. Sapporo, Japan

Kirsch (1898) Die Theorie der Elastizität und dieBedürfnisse der Festigkeitslehre. Z Ver Deutsch Ing 42(28):797–807

Martin CD, Read RS, Martino JB (1997) Observation of brittle failure around a circular test tunnel. Int J Rock Mech Min Sci 34:1065–1073

Martin CD, Kaiser PK, McCreath DR (1999) Hoek-Brown parameters for predicting the depth of brittle failure around tunnels. Can Geotech J 36:136–151

Ortlepp W (2001) The behaviour of tunnels at great depth under large static and dynamic pressures. Tunn Undergr Space Technol 16:41–48

Rocscience Inc., (2012) Phase2©, version 8.012. http://www.rocscience.com. Accessed 2019

Saurer E, Marcher T, Schaedlich B, Schweiger HF (2014) Validation of a novel constitutive model for shotcrete using data from an executed tunnel. Geomech Tunn 7(4):353–336. https://doi.org/10.1002/geot.201400023

Shaalan H, Ismail MAM, Azit R (2017) Evaluation of TBM tunnels with respect to stability against spalling. AIP Conference Proceedings

Sulem J, Panet M, Guenot A (1987) Closure analysis in deep tunnels. Int J Rock Mech Min Sci 24:145–154

Vandewalle M (1998) The use of steel fibre reinforced shotcrete for the support of mine openings. J South Afr Inst Min Metall 98(3):113–120

Yu ZH, Kulatilake PHSW, Jiang FX (2012) Effect of tunnel shape and support system on stability of a tunnel in a deep coal mine in China. Geotech Geol Eng. https://doi.org/10.1007/s10706-011-9475-0